28. Simon, C. & Irvine, W. Robust long-distance entanglement and a loophole-free Bell test with ions and photons. *Phys. Rev. Lett.* **91,** 110405 (2003).
29. Cabrillo, C., Cirac, J. I., Garcia-Fernandez, P. & Zoller, P. Creation of entangled states of distant atoms by interference. *Phys. Rev. A* **59,** 1025–1033 (1999).
30. Bennett, C. H., DiVincenzo, D. P., Smolin, J. A. & Wootters, W. K. Mixed-state entanglement and quantum error correction. *Phys. Rev. A* **54,** 3824–3851 (1996).

Acknowledgements We acknowledge discussions with M. Madsen, P. Haljan, M. Acton and D. Wineland, and thank R. Miller for assistance in building the trap apparatus. This work was supported by the National Security Agency, the Advanced Research and Development Activity, under Army Research Office contract, and the National Science Foundation Information Technology Research Division.

Competing interests statement The authors declare that they have no competing financial interests.

Correspondence and requests for materials should be addressed to B.B. (bblinov@umich.edu).

Supramolecular dendritic liquid quasicrystals

Xiangbing Zeng[1], Goran Ungar[1], Yongsong Liu[1], Virgil Percec[2], Andrés E. Dulcey[2] & Jamie K. Hobbs[3]

[1]*Department of Engineering Materials, University of Sheffield, Sheffield S1 3JD, UK*
[2]*Roy & Diana Vagelos Laboratories, Department of Chemistry, University of Pennsylvania, Philadelphia, Pennsylvania 19104-6323, USA*
[3]*H. H. Wills Physics Laboratory, University of Bristol, Bristol BS8 1TL, UK*

A large number of synthetic and natural compounds self-organize into bulk phases exhibiting periodicities on the 10^{-8}–10^{-6} metre scale[1] as a consequence of their molecular shape, degree of amphiphilic character and, often, the presence of additional non-covalent interactions. Such phases are found in lyotropic systems[2] (for example, lipid–water, soap–water), in a range of block copolymers[3] and in thermotropic (solvent-free) liquid crystals[4]. The resulting periodicity can be one-dimensional (lamellar phases), two-dimensional (columnar phases) or three dimensional ('micellar' or 'bicontinuous' phases). All such two- and three-dimensional structures identified to date obey the rules of crystallography and their symmetry can be described, respectively, by one of the 17 plane groups or 230 space groups. The 'micellar' phases have crystallographic counterparts in transition-metal alloys, where just one metal atom is equivalent to a $10^3 - 10^4$-atom micelle. However, some metal alloys are known to defy the rules of crystallography and form so-called quasicrystals, which have rotational symmetry other than the allowed two-, three-, four- or six-fold symmetry[5]. Here we show that such quasiperiodic structures can also exist in the scaled-up micellar phases, representing a new mode of organization in soft matter.

Research on bulk nanoscale self-assembly of organic matter is partly motivated by the fact that such complex structures may serve as scaffolds for photonic materials[6] and other nanoarrays, or as precursors for mesoporous ceramics or elements for molecular electronics. Larger biological objects, such as cylinder-like or sphere-like viruses, also pack on similar macrolattices[7].

Dendrons and dendrimers (tree-like molecules[8]) are proving particularly versatile in generating periodic nanostructures (Fig. 1). Two micellar lattices, with space groups $Im\bar{3}m$ (body-centred cubic, b.c.c.)[9], and $Pm\bar{3}n$ (refs 10, 11), have been established. An analogue of the $Im\bar{3}m$ phase has also been observed in block copolymers[12], and that of the $Pm\bar{3}n$ phase in lyotropic liquid crystals[13]. Recently, a complex three-dimensional (3D) tetragonal lattice (space group $P4_2/mnm$) was found, having 30 self-assembled micelles in the unit cell (Fig. 1f)[14].

In many dendron systems, thermal transitions between the phases in Fig. 1 occur. The master sequence $\mathrm{Col_h} \rightarrow Pm\bar{3}n \rightarrow P4_2/mnm \rightarrow Im\bar{3}m$ is obeyed with increasing temperature; in only a handful of cases are all these phases displayed in the same material. In a number of compounds, however, an additional unidentified phase has been observed below any other 3D phase but above $\mathrm{Col_h}$. A small-angle X-ray powder diffractogram of this phase, recorded on dendron **I** (Fig. 1g), is shown in Fig. 2a. The synthesis of **I** is described in ref. 15 and Supplementary Information, where this compound is labelled $[3,4,5\text{-}(3,5)^2]12G_3CH_2OH$. Other compounds that show the X-ray signature of this phase include $(4\text{-}3,4,5\text{-}3,5)12G_2CH_2OH$, $[4\text{-}(3,4,5)^2]12G_2COOH$, $[3,4\text{-}(3,5)^2]12G_3COOH$, $[3,4\text{-}(3,5)^2]12G_3CH_2OH$, $[3,4\text{-}(3,4,5)^2]12G_3CH_2OH$ (ref. 15), polyoxazolines with tapered side groups containing alkyl chains of different lengths[16], as well as certain salts of 3,4,5-*tris*-(*n*-alkoxy)benzoic acid[17].

On heating, compound **I** shows the following phase sequence: room temperature $\rightarrow$X$\rightarrow$ 71 °C$\rightarrow P4_2/mnm \rightarrow$ 72 °C$\rightarrow$ isotropic liquid, while on cooling phase X forms directly from the liquid (Supplementary Information). This allowed us to grow mono-domains of the unknown phase. That phase X is a quasicrystal is revealed by the distinctive but crystallographically forbidden 12-fold symmetry of the small-angle X-ray single-crystal pattern (Fig. 2b). When the sample is rotated around the 12-fold axis with the incident beam perpendicular to the axis, the diffraction pattern repeats every 30°. One such pattern is shown in Fig. 2c, where the Ewald sphere cuts through a pair of strong reflections in Fig. 2b. The structure of this liquid quasicrystal (LQC) is periodic in the direction of the 12-fold axis, but quasiperiodic in the plane perpendicular to it.

In contrast to normal 3D periodic structures, five instead of three basis vectors are needed for indexing the diffraction peaks of a dodecagonal quasicrystal[18]. Four of the vectors, $\mathbf{q}^1$, $\mathbf{q}^2$, $\mathbf{q}^3$ and $\mathbf{q}^4$,

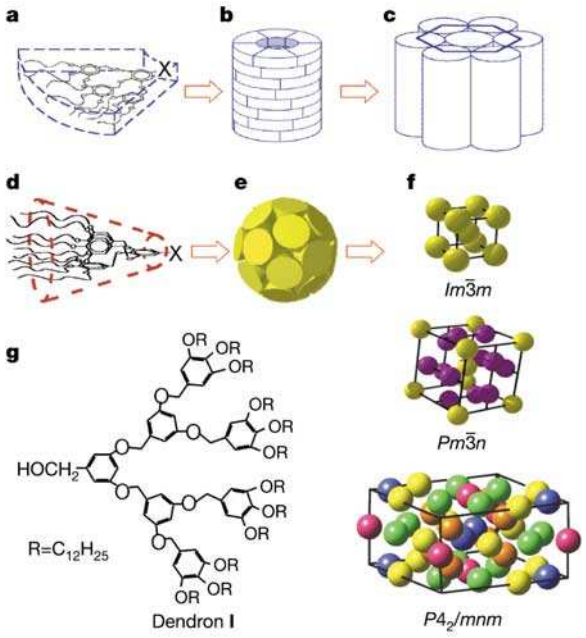

Figure 1 Self-assembly of wedge-shaped molecules. **a**, Dendrons with fewer tethered chains adopt a flat slice-like shape (X is a weakly binding group). **b**, The slices stack up and form cylindrical columns, which assemble on a two-dimensional hexagonal columnar ($\mathrm{Col_h}$) lattice (**c**). **d**, Dendrons with more end-chains assume a conical shape. **e**, The cones assemble into spheres, which pack on three different 3D lattices (**f**) with symmetries $Im\bar{3}m$, $Pm\bar{3}n$ and $P4_2/mnm$. **g**, Structure of compound **I** studied in this work.

are perpendicular to the 12-fold axis (Fig. 2b). $\mathbf{q}^5$, along the 12-fold axis, is indicated in Fig. 2c. Thus each diffraction peak $\mathbf{q}$ is indexed by five integers ($n^1n^2n^3n^4$ and n^5) where $\mathbf{q} = \Sigma_{i=1}^{5} n^i\mathbf{q}^i$. Tentative indices of some of the diffraction peaks are given in Fig. 2.

The structure of the LQC is closely related to those of the $Pm\bar{3}n$ and $P4_2/mnm$ phases. Where these phases form from the LQC on heating, their {002} reflections appear at the same position as the {00002} reflections of the LQC. Thus the periodicity of the LQC along the 12-fold axis is the same as that of $Pm\bar{3}n$ along any of the three cubic axes, and $P4_2/mnm$ along c. This suggests that, like the above phases, the LQC is also micellar. With increasing temperature, the observed d-spacings of the LQC decrease proportionally. This isotropic shrinkage suggests a phase containing isometric objects.

$Pm\bar{3}n$, $P4_2/mnm$ and $Im\bar{3}m$ (b.c.c.) phases that are observed in dendrimers all have their structural equivalents in transition metals or alloys (for example, $Pm\bar{3}n$: Cr_3Si; $P4_2/mnm$: $Fe_{46}Cr_{54}$ and β-uranium; b.c.c.: α-iron). The dendrimer 'atoms' (micelles) have volumes several thousand times larger than real atoms, and so do their unit cells. Both $Pm\bar{3}n$ and $P4_2/mnm$ phases belong to the family of tetrahedrally close packed (t.c.p.) structures of spherical objects, or Frank–Kasper phases[19]. In a t.c.p. structure, any four neighbouring spheres pack tetrahedrally, which is locally the densest packing. However, regular tetrahedral interstices are incompatible with long-range order. Such frustration leads to the complexity of

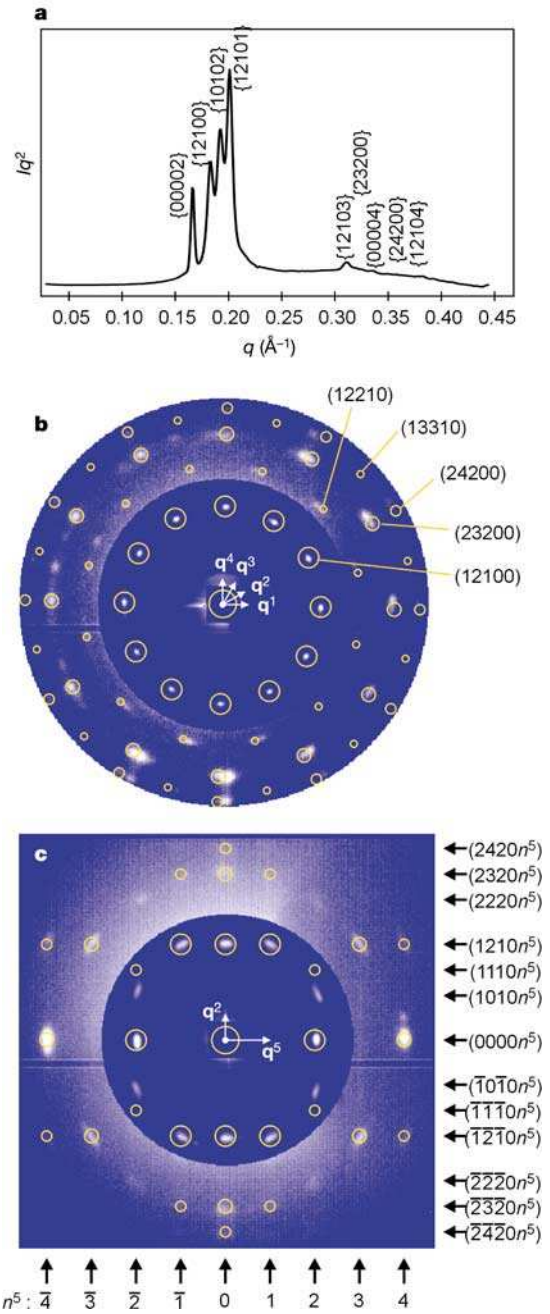

Figure 2 Experimental and simulated X-ray diffraction patterns of the LQC. **a**, Powder diffraction pattern of compound **I** recorded at 70 °C. **b**, Precession single-crystal pattern along the 12-fold axis. The intensities of outer diffraction peaks in **b** and **c** are scaled up by 100. **c**, Single-crystal diffraction pattern perpendicular to the 12-fold axis, cutting through one of the six pairs of strong diffraction spots in **b**. The pattern repeats itself every 30° when the sample is rotated around the 12-fold axis. All single-crystal patterns were recorded at room temperature. Simulated diffraction patterns are superimposed, with the reflections represented by circles whose area is proportional to log(amplitude). The apparent deviation in position of diffraction spots in the outer region of the diffraction pattern in **c** is due to the existence of other domains in the sample (see Supplementary Information).

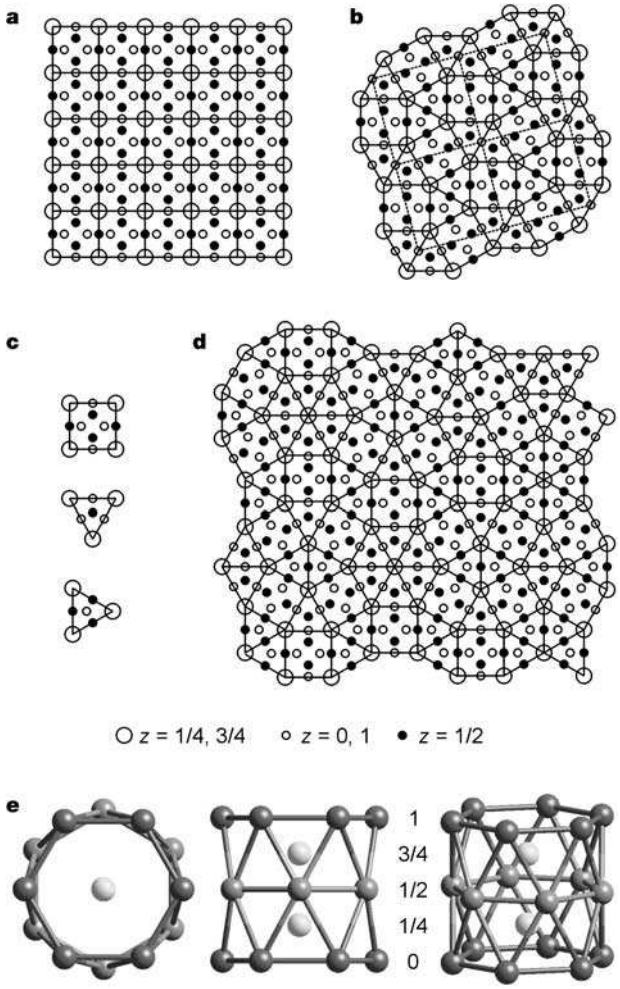

Figure 3 Packing of spheres in the LQC and other related t.c.p. structures. All can be generated from 2D tilings consisting of only squares and equilateral triangles ('sparse' nets, elevations $z = 1/4$ and 3/4, large open circles). These tiles are 'decorated' with spheres at $z = 0$ (small open circles) and 1/2 (filled circles), forming the 'dense' nets. **a**, Sphere packing in $Pm\bar{3}n$. **b**, Sphere packing in $P4_2/mnm$. **c**, Only three different decorated tiles, one square and two triangular, are used to generate both $Pm\bar{3}n$ and $P4_2/mnm$ structures. **d**, The same tiles, when arranged quasiperiodically, will generate the model of the LQC with 12-fold symmetry. The lattice constant, that is, the length of the tile edge, as well as the periodicity along the 12-fold axis, is 81.4 Å at room temperature. **e**, Two ideal hexagonal antiprisms stacked along the $\overline{12}$ symmetry axis. There is a distorted hexagonal antiprism at each node of the square-triangular tiling in **a**, **b** and **d**.

t.c.p. structures. Ultimately, it leads to quasicrystals.

Dodecagonal quasicrystals have been found so far in five transition-metal systems[20–23]. In all but one case, dodecagonal structures were studied by electron microscopy or electron diffraction. The interpretation of electron diffraction is complicated by multiple scattering. In the one case where quasicrystals sufficiently large for single-crystal X-ray diffraction were obtained, the stacking along the 12-fold axis was different from that in other dodecagonal phases, including the present LQC[23]. As X-ray data can be compared with models more unequivocally than electron diffraction data, we proceed to construct a model of the LQC. We follow the idea that dodecagonal structures can be generated by appropriate 'decoration' of a quasiperiodic square-triangular tiling[18,21,23].

$Pm\bar{3}n$ and $P4_2/mnm$ structures are characterized by alternating densely and sparsely populated layers, as shown in Fig. 3a and b, respectively. The nets generated by connecting the nearest neighbours in the sparsely populated layers (large circles) are equivalent to tilings that cover an infinite plane using only squares and equilateral triangles. The full 3D crystal structure is then generated by 'decoration', that is, by associating with each tile a column, periodic along *c*, containing individual micelles. Only three kinds of tiles, one square and two triangular (Fig. 3c), are needed to construct the $Pm\bar{3}n$ and $P4_2/mnm$ structures. (In the actual $P4_2/mnm$ phase, the position of the micelles is somewhat different from those in an idealized structure made up of decorated tiles (Fig. 3c). Similarly, it is expected that in the real quasicrystal, the micelles would also be somewhat away from the ideal positions assumed by our starting model (Fig. 3d)).

Using quasiperiodic tiling, the same elements can be used to construct models of the LQC (Fig. 3d). For ways of generating such tilings, see refs 24 and 25. Such models readily explain the 12-fold symmetry, and the equal periodicities in the third dimension for the LQC, $Pm\bar{3}n$ and $P4_2/mnm$ phases. Simulated diffraction patterns based on the quasiperiodic square-triangular tiling of ref. 25 are superimposed on the experimental ones in Fig. 2b and c (for details of the simulation, see Supplementary Information). Even the unrefined starting model gives a reasonable explanation of the positions and relative intensities of experimental diffraction spots (Fig. 2b and c). Nevertheless, discrepancies in intensities remain (for example, {10102} and {22202} reflections are stronger than expected). Improvement of the model is progressing, as the reliability of acquired diffraction data allows it.

Atomic force microscope images of the LQC phase on glass show that the structure is periodic in one direction but not in the other, in agreement with a quasicrystalline structure where the 12-fold axis lies parallel to the glass surface. Moreover, they support the 'micellar' nature and the layered structure of the LQC (Supplementary Information).

To explain why spherical aggregates of dendrons pack on different 3D lattices, mathematical functions defining molecular shapes ideally suited to typical lattices have been calculated[14]. In a different approach[26], micelles were approximated by hard cores and soft alkyl coronas. Assuming that thermal transitions are primarily driven by the laterally expanding alkyl chains, the first micellar phase to which a columnar dendrimer would transform on heating is expected to be the one with the minimal coronal surface area. Such a structure ought to coincide with the solution of the Kelvin problem of the ultimate equilibrium dry foam (minimum surface area per bubble). The b.c.c. structure proposed by Kelvin[27] was challenged only recently by a calculation showing that the $Pm\bar{3}n$ structure provides a better solution[28]. The fact that, of all known micellar phases in self-assembled dendrimers, the $Pm\bar{3}n$ was always found at the lowest temperature was taken as experimental vindication of the new minimal surface solution[26]. However, now that the updated phase sequence is $\mathrm{Col_h} \rightarrow \mathrm{LQC} \rightarrow Pm\bar{3}n \rightarrow P4_2/mnm \rightarrow$ b.c.c., the possibility is raised of dodecagonal quasicrystals providing a still better solution of the Kelvin problem.

Outside metal-based systems, non-crystallographic rotational symmetry has been observed only in thin films of smectic C twist grain boundary (TGBC) liquid crystals confined between glass plates with rubbed surfaces[29,30]. *q*-fold symmetry is created by helical packing of smectic C grains, and lock-in transitions between different *q*-values were observed with changing temperature. In contrast, the present LQC is a bulk phase with intrinsic high-level quasiperiodic order inherent in the molecular architecture.

The tiling of planes normal to the 12-fold axis in the LQC (Fig. 3d) can be understood intuitively in the following way. There are six tetrahedrons packed around the vertical line connecting the two light-grey spheres at $z = 1/4$ and 3/4 in Fig. 3e, taking two adjacent spheres at $z = 1/2$ as the other two tetrahedral apices. However, the number of perfect tetrahedrons that can fit around a common edge is 5.1. In different t.c.p. structures, including LQC, the inability to cover a flat surface with regular pentagons is resolved in different tilings of distorted hexagons. The problem is reversed in the case of curved surfaces; these cannot be tiled exclusively by hexagons. Thus in 'buckyballs' and footballs, a certain proportion of pentagons is required and, as the curvature radius decreases relative to tile size, this proportion increases until the all-pentagonal icosahedron is reached. Interesting examples are found in hexagonal and pentagonal packing modes of proteins in capsids (coats) of cylindrical and spherical viruses[31].

Finally, the unusual symmetry of quasicrystals has been exploited in recent years for fabrication of photonic bandgap arrays. Owing to their high symmetry, two-dimensional (2D) quasicrystalline lattices are able to induce and widen the photonic bandgap[32], preventing light within a range of wavelengths from propagating in any direction. More recently it was shown that light can be slowed down in a one-dimensional photonic quasicrystal that follows the Fibonacci sequence. To produce photonic 'quasicrystals' with photonic bandgaps in the visible light region, the distance of two neighbouring objects must be on the scale of several hundred nanometres. Whereas the results presented here show how the characteristic length of a self-assembled quasicrystal can be scaled up from a few ångströms in metal alloys to nearly 10 nm in supramolecular dendrimers, it may be possible to achieve a further increase of two orders of magnitude by using appropriately designed self-assembling dendrons, block copolymers or other soft sphere systems. □

Received 23 October 2003; accepted 26 January 2004; doi:10.1038/nature02368.

1. Supramolecular chemistry and self-assembly . *Science* **295** (special issue), 2395–2421 (2002).
2. Seddon, J. M. Lyotropic phase behaviour of biological amphiphiles. *Ber. Bunsenges. Phys. Chem.* **100,** 380–393 (1996).
3. Thomas, E. L., Anderson, D. M., Henkee, C. S. & Hoffman, D. Periodic area-minimizing surfaces in block copolymers. *Nature* **334,** 598–601 (1988).
4. Tschierske, C. Micro-segregation, molecular shape and molecular topology partners for the design of liquid crystalline materials with complex mesophase morphologies. *J. Mater. Chem.* **11,** 2647–2671 (2001).
5. Janot, C. *Quasicrystals: A Primer* (Oxford Univ. Press, Oxford, 1992).
6. Lopes, W. A. & Jaeger, H. M. Hierarchical self-assembly of metal nanostructures on diblock copolymer scaffolds. *Nature* **414,** 735–738 (2001).
7. Horne, R. W. in *Molecular Plant Virology* Vol. 1 (ed. Davies, J. W.) 1–41 (CRC, Boca Raton, 1985).
8. Newkome, G. R., Moorefield, C. N. & Vogtle, F. *Dendrimers and Dendrons* (Wiley-VCH, Weinheim, 2001).
9. Yeardley, D. J. P., Ungar, G., Percec, V., Holerca, M. N. & Johansson, G. Spherical supramolecular minidendrimers self-organized in an "inverse micellar"-like thermotropic body-centered cubic liquid crystalline phase. *J. Am. Chem. Soc.* **122,** 1684–1689 (2000).
10. Balagurusamy, V. S. K., Ungar, G., Percec, V. & Johansson, G. Rational design of the first spherical supramolecular dendrimers self-organized in a novel thermotropic cubic liquid-crystalline phase and the determination of their shape by X-ray analysis. *J. Am. Chem. Soc.* **119,** 1539–1555 (1997).
11. Hudson, S. D. *et al.* Direct visualization of individual cylindrical and spherical supramolecular dendrimers. *Science* **278,** 449–452 (1997).
12. Bates, F. S., Cohen, R. E. & Berney, C. V. Small-angle neutron scattering determination of macrolattice structure in a polystyrene polybutadiene diblock co-polymer. *Macromolecules* **15,** 589–592 (1982).
13. Luzzati, V., Vargas, R., Mariani, P., Gulik, A. & Delacroix, H. Cubic phases of lipid-containing systems—Elements of a theory and biological connotations. *J. Mol. Biol.* **229,** 540–551 (1993).
14. Ungar, G., Liu, Y. S., Zeng, X. B., Percec, V. & Cho, W.-D. Giant supramolecular liquid crystal lattice. *Science* **299,** 1208–1211 (2003).
15. Percec, V., Cho, W.-D., Ungar, G. & Yeardley, D. J. P. Synthesis and structural analysis of two

constitutional isomeric libraries of AB_2-based monodendrons and supramolecular dendrimers. *J. Am. Chem. Soc.* **123,** 1302–1315 (2001).
16. Percec, V., Holerca, M. N., Uchida, S., Yeardley, D. J. P. & Ungar, G. Poly(oxazoline)s with tapered minidendritic side groups as models for the design of synthetic macromolecules with tertiary structure. *Biomacromolecules* **2,** 729–740 (2001).
17. Percec, V. *et al.* Exploring and expanding the three-dimensional structural diversity of supramolecular dendrimers with the aid of libraries of alkali metals of their AB_3 minidendritic carboxylates. *Chem. Eur. J.* **8,** 1106–1117 (2002).
18. Gähler, F. in *Quasicrystalline Materials* (eds Janot, C. & Dubois, J. M.) 272–284 (World Scientific, Singapore, 1988).
19. Frank, F. C. & Kasper, J. S. Complex alloy structures regarded as sphere packing. I. Definitions and basic principles. *Acta Crystallogr.* **11,** 184–190 (1958).
20. Ishimasa, T., Nissen, H.-U. & Fukano, Y. New ordered state between crystalline and amorphous in Ni-Cr particles. *Phys. Rev. Lett.* **55,** 511–513 (1985).
21. Chen, H., Li, D. X. & Kuo, K. H. New type of two-dimensional quasicrystal with twelvefold rotational symmetry. *Phys. Rev. Lett.* **60,** 1645–1648 (1988).
22. Yoshida, K., Yamada, T. & Taniguchi, Y. Long-period tetragonal lattice formation by solid-state alloying at the interfaces of Bi-Mn double-layer thin-films. *Acta Crystallogr. B* **45,** 40–45 (1989).
23. Conrad, M., Krumeich, F. & Harbrecht, B. A dodecagonal quasicrystalline chalcogenide. *Angew. Chem. Int. Edn Engl.* **37,** 1383–1386 (1998).
24. Stampfli, P. A dodecagonal quasiperiodic lattice in two dimensions. *Helv. Phys. Acta* **59,** 1260–1263 (1986).
25. Baake, M., Klitzing, R. & Schlottmann, M. Fractally shaped acceptance domains of quasiperiodic square-triangle tilings with dodecagonal symmetry. *Physica A* **191,** 554–558 (1992).
26. Ziherl, P. & Kamien, R. D. Maximizing entropy by minimizing area: Towards a new principle of self-organization. *J. Phys. Chem. B* **105,** 10147–10158 (2001).
27. Thomson, W. On the division of space with minimum partitional area. *Phil. Mag.* **24,** 503–514 (1887).
28. Weaire, D. (ed.) *The Kelvin Problem: Foam Structures of Minimal Surface Area* (Taylor & Francis, London, 1997).
29. Navailles, L., Barois, P. & Nguyen, H. T. X-ray measurement of the twisted grain boundary angle in the liquid crystal analog of the Abrikosov phase. *Phys. Rev. Lett.* **71,** 545–548 (1993).
30. Navailles, L., Pindak, R., Barois, P. & Nguyen, H. T. Structural study of the smectic-C twisted grain boundary phase. *Phys. Rev. Lett.* **74,** 5224–5227 (1995).
31. Bruinsma, R. F., Gelbart, W. M., Reguera, D., Rudnick, J. & Zandi, R. Viral self-assembly as a thermodynamic process. *Phys. Rev. Lett.* **24,** 248101 (2003).
32. Zoorob, M. E., Charlton, M. D. B., Parker, G. J., Baumberg, J. J. & Netti, M. C. Complete photonic bandgaps in 12-fold symmetric quasicrystals. *Nature* **404,** 740–743 (2000).

Supplementary Information accompanies the paper on **www.nature.com/nature**.

Acknowledgements We thank A. Gleeson and P. Baker for assistance with X-ray diffraction experiments. We are grateful to P. A. Heiney, T. C. Lubensky and R. D. Kamien for reading the draft manuscript and for their suggestions. We acknowledge CCLRC for providing synchrotron beamtime. The synthesis part of the work was supported by the NSF.

Competing interests statement The authors declare that they have no competing financial interests.

Correspondence and requests for materials should be addressed to G.U. (g.ungar@sheffield.ac.uk).

Links between salinity variation in the Caribbean and North Atlantic thermohaline circulation

Matthew W. Schmidt[1], Howard J. Spero[1] & David W. Lea[2]

[1]*Department of Geology, University of California, Davis, California 95616, USA*
[2]*Department of Geological Sciences and Marine Science Institute, University of California, Santa Barbara, California 93106, USA*

Variations in the strength of the North Atlantic Ocean thermohaline circulation have been linked to rapid climate changes[1] during the last glacial cycle through oscillations in North Atlantic Deep Water formation and northward oceanic heat flux[2–4]. The strength of the thermohaline circulation depends on the supply of warm, salty water to the North Atlantic, which, after losing heat to the atmosphere, produces the dense water masses that sink to great depths and circulate back south[2]. Here we analyse two Caribbean Sea sediment cores, combining Mg/Ca palaeothermometry with measurements of oxygen isotopes in foraminiferal calcite in order to reconstruct tropical Atlantic surface salinity[5,6] during the last glacial cycle. We find that Caribbean salinity oscillated between saltier conditions during the cold oxygen isotope stages 2, 4 and 6, and lower salinities during the warm stages 3 and 5, covarying with the strength of North Atlantic Deep Water formation[7]. At the initiation of the Bølling/Allerød warm interval, Caribbean surface salinity decreased abruptly, suggesting that the advection of salty tropical waters into the North Atlantic amplified thermohaline circulation and contributed to high-latitude warming.

Today, most of the North Atlantic's subtropical gyre water circulates through the Caribbean Sea before it is transported to the subpolar regions of the North Atlantic via the Gulf Stream[8]. Net evaporation exceeds precipitation in the Atlantic, resulting in freshwater removal of $\sim 0.35 \times 10^6\ m^3\ s^{-1}$ from the Atlantic basin[9]. Because of their influence on North Atlantic surface salinity, the tropical and subtropical Atlantic play an important part in regulating North Atlantic Deep Water (NADW) formation. However, unlike the Gulf of Mexico and North Atlantic, Caribbean salinity is not significantly affected by freshwater runoff and therefore surface salinity primarily reflects the evaporation/precipitation ratio over the western tropical Atlantic. Hence, changes in tropical

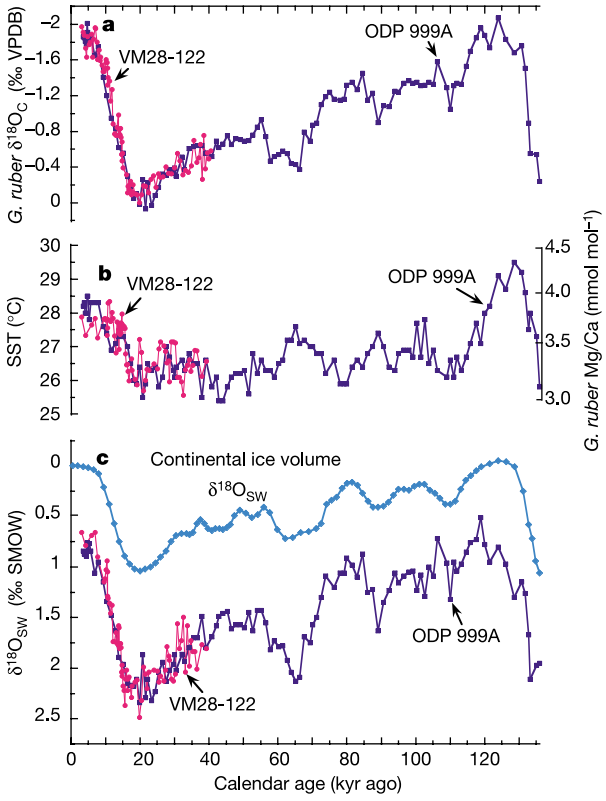

Figure 1 Temperature and $\delta^{18}O_{SW}$ variation in the western Caribbean Sea during the past 136 kyr. **a**, Colombian basin $\delta^{18}O_C$ and **b**, Mg/Ca–SST records from ODP 999A (12° 45′ N, 78° 44′ W; 2,827 m; 4 cm kyr^{-1} sedimentation rate) and VM28-122 (11° 34′ N, 78° 25′ W; 3,623 m; 4 cm kyr^{-1} sedimentation rate during the Holocene and LGM, 10–15 cm kyr^{-1} sedimentation rate during the deglaciation), based on the planktic foraminifer *G. ruber* (white). Mg/Ca was converted to SST[13] using Mg/Ca = 0.38exp0.09[SST–0.61(core depth, in km)]. **c**, Computed $\delta^{18}O_{SW}$ calculated from the Mg/Ca-derived SST and $\delta^{18}O_C$ using T (in °C) = 16.5 − 4.80 (δ_C − (δ_W − 0.27)) (ref. 14). The continental ice-volume $\delta^{18}O_{SW}$ reconstruction[15] is shown for comparison. Note that the amplitude of the calculated $\delta^{18}O_{SW}$ change in the Colombian basin is considerably greater than the global $\delta^{18}O_{SW}$ change due to ice volume alone.